1
Introduction

This chapter provides an introduction to the subject known as gradient-index optics. Section 1.1 provides a historical perspective on this subject before introducing the essential concepts needed in later chapters. Section 1.2 is devoted to various types of refractive-index profiles that are employed for making gradient-index devices, with particular emphasis to the parabolic index profile because of its practical importance. In Section 1.3, we discuss the relevant properties of such devices such as optical losses, chromatic dispersion, and intensity dependence of the refractive index occurring at high power levels. The focus of Section 1.4 is on the materials and the techniques used for fabricating gradient-index devices in the form of a rod or a thin fiber. Section 1.5 provides an overview of how the book is organized for presenting a wide body of research carried out during the last 50 years in the area of gradient-index optics.

1.1 Historical Perspective

Propagation of electromagnetic radiation in any medium is affected by its refractive index, denoted as $n(\mathbf{r}, \omega)$ because of its dependence on the frequency ω of the radiation and on the location $\mathbf{r}$ within the medium. In the case of a homogeneous material with uniform density, the dependence of $n(\mathbf{r}, \omega)$ on $\mathbf{r}$ can be ignored. However, the $\mathbf{r}$ dependence of the refractive index must be considered when density variations occur, either naturally (such as in air) or are introduced artificially by grading the refractive index of a material in some fashion. As an example, the phenomenon of mirage results from an index gradient formed in air on a hot day. Such index gradients change with time because of changes in air's temperature and pressure. When density variations in a medium are static (time independent), the medium is referred to as a graded-index (GRIN) medium. We only consider static density variations in this book.

https://doi.org/10.1017/9781009282086.002 Published online by Cambridge University Press

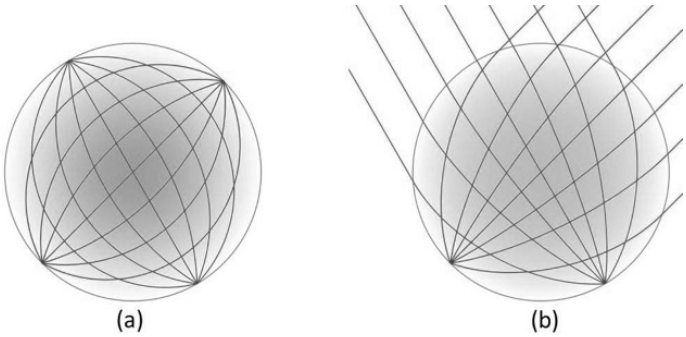

Figure 1.1 Schematic illustration of the GRIN lenses proposed by (a) Maxwell and (b) Luneberg. In both cases, refractive index is the largest at the center and decreases radially toward's the sphere's surface.

Historically, Maxwell proposed more than 160 years ago the concept of a GRIN device, known as the fisheye lens, even before he developed his celebrated equations [1]. The refractive index for such a lens exhibits spherical symmetry and depends on the magnitude of the vector **r**, but not on its direction. Similar ideas were used by Wood [2] in 1906, and by Luneberg in 1954, for imaging applications [3]. Figure 1.1 shows schematically how optical rays bend because of changes in the refractive index inside the GRIN lenses proposed by Maxwell and Luneberg. In both cases, optical rays follow curved paths to come to focus at a point on the sphere's surface.

With advances in glass technology, GRIN glasses could be fabricated by 1970 in which the refractive index varied in a cylindrically symmetric fashion in the plane normal to the direction of propagation. Such GRIN glasses were used either in a rod form [4] or drawn into a fiber form [5], depending on the application. At the same time, planar waveguides were developed in which the refractive index $n(x)$ varied only in one direction normal to the direction of propagation [6–8]. Two books published around 1977 provided a comprehensive account of such GRIN devices [9, 10].

The GRIN fibers were developed during the 1970s and their properties studied extensively in view of their potential applications in the emerging area of optical communications [11]. Indeed, by the year 1980, GRIN fibers were used for the first generation of such systems [12]. Even though telecommunication systems began using single-mode, step-index fibers by 1985, the development of new GRIN materials and devices remained an active area of research. For example, plastic-based GRIN fibers are used routinely for data-transfer applications [13]. One can get a good idea of the intense activity during the 1980s and 1990s by consulting several special issues of the *Applied Optics* journal [14]. Two books also describe the progress realized during this period [15, 16].

https://doi.org/10.1017/9781009282086.002 Published online by Cambridge University Press

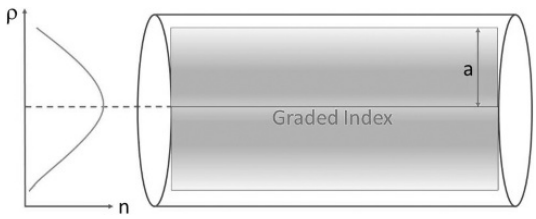

Figure 1.2 Schematic illustration of the refractive-index gradient along a GRIN device.

Starting around 2010, the advent of space-division multiplexing for modern telecommunication systems led to a renewed interest in the use of glass-based GRIN fibers [12, 17, 18]. Since then, the investigation of nonlinear optical phenomena in GRIN fibers has led to major advances. Among these are the topics such as spatiotemporal modulation instability, GRIN solitons, and spatial beam cleanup [19–21]. This book is intended to cover recent research advances and to provide, at the same time, comprehensive coverage of electromagnetic wave propagation inside a GRIN medium.

1.2 Refractive-Index Profiles

The focus of this book is on a GRIN medium whose refractive index varies in a plane normal to the direction of propagation (commonly taken to be the z axis) in a cylindrically symmetric fashion. Figure 1.2 shows schematically how the refractive index varies in such a GRIN rod around its central axis, chosen to be the z axis of the coordinate system. For practical reasons, the refractive index is the largest at the central axis and decreases gradually in all radial directions moving away from the center. In its most general form, the refractive index varies with the radial distance $\rho = \sqrt{x^2 + y^2}$ as [22–24]

$$n^2(\rho) = \begin{cases} n_0^2[1 - 2\Delta f(\rho/a)] & (0 \le \rho \le a) \\ n_0^2(1 - 2\Delta) = n_c^2 & (\rho \ge a), \end{cases} \tag{1.2.1}$$

where n_0 is the maximum value of the refractive index at the center and n_c is its minimum value at $\rho = a$, which is the radius of the cylindrical core enclosing the GRIN region. The function $f(x)$ governs shape of the index profile such that its value is 1 for $x = 1$.

The parameter Δ can be deduced from Eq. (1.2.1) and has the form

$$\Delta = \frac{n_0^2 - n_c^2}{2n_0^2} \approx \frac{n_0 - n_c}{n_0}. \tag{1.2.2}$$

https://doi.org/10.1017/9781009282086.002 Published online by Cambridge University Press

where the approximate form holds when n_c differs from n_0 by at most a few percent so that $\Delta \ll 1$. This is often the case in practice for most GRIN devices. Using $\Delta \ll 1$, the refractive index in Eq. (1.2.1) can be approximated as

$$n(\rho) \approx \begin{cases} n_0[1 - \Delta f(\rho/a)] & (0 \le \rho \le a) \\ n_0(1 - \Delta) = n_c & (\rho > a). \end{cases} \tag{1.2.3}$$

This equation shows that $n(\rho)$ decreases as one moves away from the central axis up to a distance $\rho = a$ in a fashion dictated by the function $f(\rho)$ and takes minimum value n_c in the cladding region $\rho > a$. The GRIN region of radius a constitutes the core of such a GRIN device. The parameter Δ, given in Eq. (1.2.2), represents the fractional decrease in the refractive index across the core and its value is a design parameter for GRIN devices.

The function $f(x)$ governs the shape of the index profile for a GRIN device. This shape depends on the application for which the device is fabricated for and can vary over a wide range. In the case of planar waveguides, even an error function has been used for the shape [8]. In the case of GRIN rods and fibers, it is common to employ a power-law index profile with $f(x) = x^p$, where the exponent p governs the shape of the GRIN region. In this case, the refractive index in the core region varies as [22–24]

$$n^2(\rho) = n_0^2\Big[1 - 2\Delta\Big(\frac{\rho}{a}\Big)^p\Big] \qquad (\rho \le a). \tag{1.2.4}$$

Figure 1.3 shows how the refractive-index profile changes when p is varied in the range 1–10 using $n_0 = 1.5$ and $\Delta = 0.06$. The case $p = 2$ corresponds to a parabolic shape of the index profile. Note that the shape becomes closer to a step function for a large value of p such that n remains close to n_0 until one approaches the region near $\rho = a$, where it decreases rapidly and takes the value n_c. A step-index profile, occurring in the limit $p \to \infty$, is used routinely for making step-index fibers. Its use confines light within the core of a step-index fiber through the phenomenon of total internal reflection.

A parabolic index profile, realized for the choice $p = 2$ in Eq. (1.2.4), plays an important role in the literature on GRIN media, and many GRIN devices are designed with such a profile. In this case, we can write Eq. (1.2.4) in the simple form

$$n^2(\rho) = n_0^2(1 - b^2\rho^2), \qquad b = \sqrt{2\Delta}/a. \tag{1.2.5}$$

The parameter b is a measure of the index gradient such that its larger values indicate a faster reduction in the refractive index as ρ is increased. This parameter will play a prominent role in later chapters. As seen from the definition of b in Eq. (1.2.5), its value depends both on the core's radius a and the relative index difference Δ.

Depending on the application, numerical values of the three parameters, a, n_0, and Δ, associated with a GRIN device can vary over a wide range. We classify

https://doi.org/10.1017/9781009282086.002 Published online by Cambridge University Press

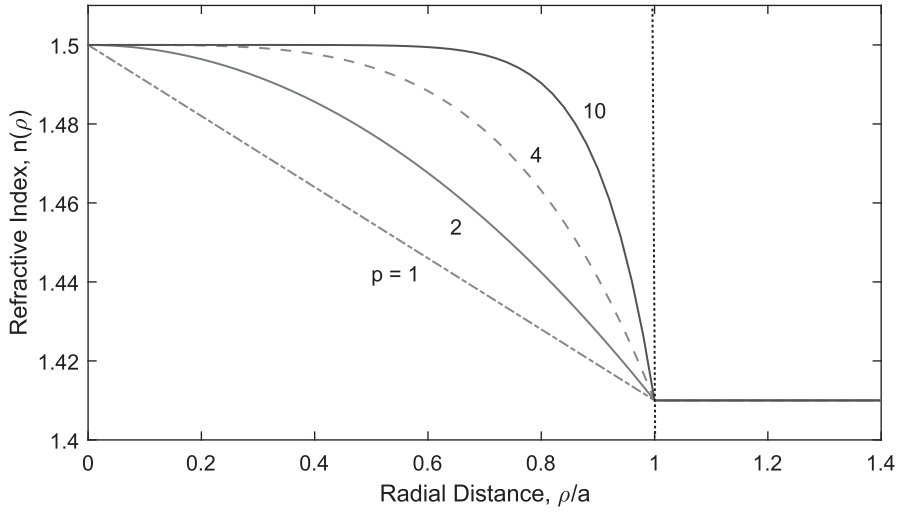

Figure 1.3 Refractive index $n(\rho)$ plotted as a function of the ratio ρ/a for several values of the parameter p. The vertical dotted line at $\rho = a$ separates the core and cladding regions of such GRIN devices.

GRIN devices into two broad groups based on the core's radius a. The value of a exceeds 1 mm for GRIN rods used to make lenses and similar optical elements. In contrast, a is restricted to much smaller values in the range of 10–30 μm for GRIN fibers used for telecommunication applications, among other things. The parameter Δ also varies for these two groups of GRIN devices. Its typical value is around 0.01 for GRIN fibers but can exceed 0.05 for GRIN rods. The value of n_0 depends on the material used for making a GRIN device. In the case of silica glass, n_0 is about 1.45. For plastics, n_0 is closer to 1.5.

We can estimate the value of the parameter b for GRIN rods and fibers from Eq. (1.2.5) by using the values of a and Δ. For GRIN rods, typical values of b are near 0.3 mm^{-1}. In contrast, b is around 5 mm^{-1} for GRIN fibers. Another relevant parameter of a GRIN device is its numerical aperture (NA). As indicated in Section 3.1, it depends on the values of n_0 and Δ as NA $= n_0\sqrt{2\Delta}$. The NA of a GRIN rod is close to 0.5 when $n_0 = 1.5$ and $\Delta = 0.05$. It is lower for GRIN fibers and has values of 0.2 or less.

1.3 Relevant Optical Processes

All materials affect the electromagnetic radiation propagating through them. The most relevant effects are (i) loss of power with distance owing to absorption and scattering, (ii) chromatic dispersion or a frequency-dependent refractive index, and

https://doi.org/10.1017/9781009282086.002 Published online by Cambridge University Press

(iii) intensity-dependent changes in the refractive index of the material. All three are discussed in this section.

1.3.1 Power-Loss Mechanisms

Under quite general conditions, changes in the average power P of an optical beam propagating through a GRIN medium are governed by the Beer–Lambert law [25]:

$$\frac{dP}{dz} = -\alpha P, \tag{1.3.1}$$

where α is called the attenuation coefficient. It includes not only absorption of power by the material but also other sources of power attenuation such as Rayleigh scattering. If P_{in} is the power launched inside a GRIN medium of length L, the output power P_{out} is found by integrating Eq. (1.3.1) to be

$$P_{\text{out}} = P_{\text{in}} \exp(-\alpha L). \tag{1.3.2}$$

It is customary to express α in the decibel units using the relation [12]

$$\alpha\,(\text{dB/m}) = -\frac{10}{L}\log_{10}\left(\frac{P_{\text{out}}}{P_{\text{in}}}\right) \approx 4.343\alpha. \tag{1.3.3}$$

Numerical values of the attenuation coefficient α depend both on the material used to make a GRIN device and the wavelength of light launched into it. Figure 1.4 compares the wavelength dependence of measured loss in silica-glass fibers to losses in two types of plastic fibers [26]. As seen there, plastic fibers exhibit much larger losses (> 10 dB/km) compared to those of silica fibers, whose losses can be reduced to below 0.2 dB/km in the wavelength region near 1550 nm. Absorption by the plastic material is the source of high losses in plastic GRIN fibers.

In the case of optical glasses, absorption by the material of the glass is relatively small in the visible and near-infrared regions. However, even small amounts of impurities can increase this loss considerably. In the case of silica fibers, losses can be reduced to below 1 dB/km by eliminating all impurities. For such fibers, the dominant contribution to α arises from Rayleigh scattering, which is a fundamental loss mechanism arising from local microscopic fluctuations in the density of glass used to make the fiber. Glass molecules move randomly in the molten state and freeze in place during cooling. Resulting density fluctuations produce random fluctuations in the refractive index on a scale smaller than the optical wavelength λ. These fluctuations are the source of Rayleigh scattering, whose cross section varies as λ^{-4} [25]. As seen in Figure 1.4, silica's loss resulting from Rayleigh scattering exceeds 1 dB/km in the visible region but is reduced to below 0.2 dB/km in the infrared region near 1550 nm used for modern optical communication systems.

https://doi.org/10.1017/9781009282086.002 Published online by Cambridge University Press

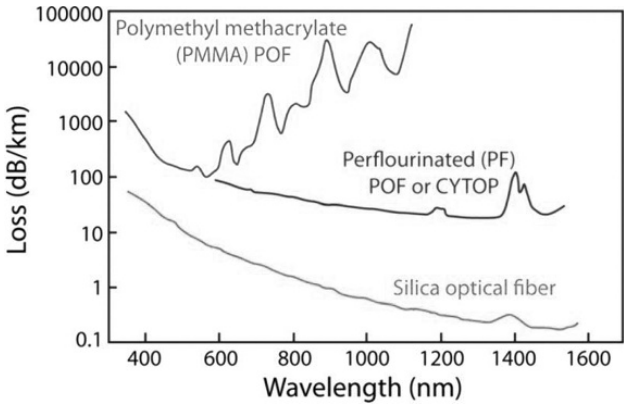

Figure 1.4 Wavelength dependence of the loss in silica fibers and losses in two types of plastic fibers. Note the logarithmic scale in units of dB/km. (After Ref. [26]; ©2014 IOP.)

1.3.2 Chromatic Dispersion

In the case of a GRIN medium, the refractive index $n(\rho, \omega)$ depends both on the spatial location ρ and the frequency ω. Chromatic dispersion has its origin in the frequency dependence of the refractive index. As we shall see in Section 2.1, it is the frequency dependence of the propagation constant, defined as $\beta(\omega) = n(\omega)(\omega/c)$, where c is the speed of light in vacuum, that governs the dispersive properties of any material. When the spectrum of incident light is narrower compared to its central frequency ω_0, we can expand $\beta(\omega)$ in a Taylor series as

$$\beta(\omega) = \beta_0 + \beta_1(\Delta\omega) + \tfrac{1}{2}\beta_2(\Delta\omega)^2 + \ldots, \tag{1.3.4}$$

where $\Delta\omega = \omega - \omega_0$ and $\beta_m = (d^m\beta/d\omega^m)_{\omega=\omega_0}$.

In Eq. (1.3.4), β_1 is related inversely to the group velocity v_g and is responsible for the group delay, $\tau_g = \beta_1 L$, over a length L. The parameter β_2, representing the second derivative of β, is called the group-velocity dispersion (GVD) parameter. This parameter will play an important role in chapters dealing with the propagation of optical pulses inside a GRIN medium. For pulses shorter than 1 ps, it is sometimes necessary to consider the cubic term containing β_3 in the Taylor series in Eq. (1.3.4). This parameter is referred to as the third-order dispersion parameter.

The dispersion parameter β_1 can be calculated for any GRIN medium by taking the frequency derivative of β as

$$\beta_1 = \frac{d\beta}{d\omega} = \frac{n_g}{c}, \qquad n_g = n + \omega\frac{dn}{d\omega}, \tag{1.3.5}$$

https://doi.org/10.1017/9781009282086.002 Published online by Cambridge University Press

where n_g is called the group index. It can be employed to calculate the GVD parameter in the form

$$\beta_2 = \frac{d\beta_1}{d\omega} = \frac{1}{c}\frac{dn_g}{d\omega}. \tag{1.3.6}$$

The sign of β_2 depends on the sign of the derivative $dn_g/d\omega$ and can be positive or negative in different spectral regions for glasses used to make a GRIN device. A related dispersion parameter D is also used for GVD; it is defined as

$$D = \frac{d\beta_1}{d\lambda} = -\frac{\lambda}{c}\frac{d^2n}{d\lambda^2}. \tag{1.3.7}$$

It is easy to show that D is related to β_2 by the relation $D = -(2\pi c/\lambda^2)\beta_2$ and its sign is opposite to that of β_2.

On a fundamental level, the origin of dispersion is related to the atomic resonance frequencies at which a material absorbs electromagnetic radiation. Far from such resonances, the refractive index is well approximated by the Sellmeier equation [27],

$$n^2(\omega) = 1 + \sum_{j=1}^{M} \frac{B_j\omega_j^2}{\omega_j^2 - \omega^2}, \tag{1.3.8}$$

where ω_j is the resonance frequency and B_j is the oscillator strength. The parameters B_j and ω_j are obtained empirically by fitting the measured dispersion curve to Eq. (1.3.8) with $M = 3$. For pure silica glass, these parameters are found to be [27] $B_1 = 0.6961663$, $B_2 = 0.4079426$, $B_3 = 0.8974794$, $\lambda_1 = 0.0684043$ μm, $\lambda_2 = 0.1162414$ μm, and $\lambda_3 = 9.896161$ μm, where $\lambda_j = 2\pi c/\omega_j$ for $j = 1$ to 3.

We can use Eq. (1.3.8) to calculate the frequency dependence of n and n_g for the silica glass without an index gradient. Figure 1.5 shows this dependence in the wavelength range 0.6–1.6 μm. The group-delay parameter is obtained using $\beta_1 = n_g/c$. Even though n decreases monotonically with λ in the entire wavelength range, β_1 exhibits a shallow minimum for silica glass at the specific wavelength, $\lambda = 1.276$ μm, marked by the dotted vertical line in Figure 1.5. This wavelength is called the zero-dispersion wavelength (denoted by λ_{ZD}) because the GVD parameter β_2 vanishes at this wavelength.

Figure 1.6 shows how the dispersion parameters β_2 and D vary with wavelength λ for silica glass (no index gradient) using Eqs. (1.3.6) and (1.3.7). As expected, both β_2 and D vanish at λ_{ZD} near 1.27 μm and change sign for longer wavelengths. It is common to refer to negative values of β_2 as the GVD being anomalous. The curve marked d_{12} shows the differential group delay, $d_{12} = \beta_1(\lambda_1) - \beta_1(\lambda_2)$, using a reference wavelength $\lambda_2 = 0.8$ μm. It shows the relative delay of a pulse as its central wavelength λ_1 is varied.

https://doi.org/10.1017/9781009282086.002 Published online by Cambridge University Press

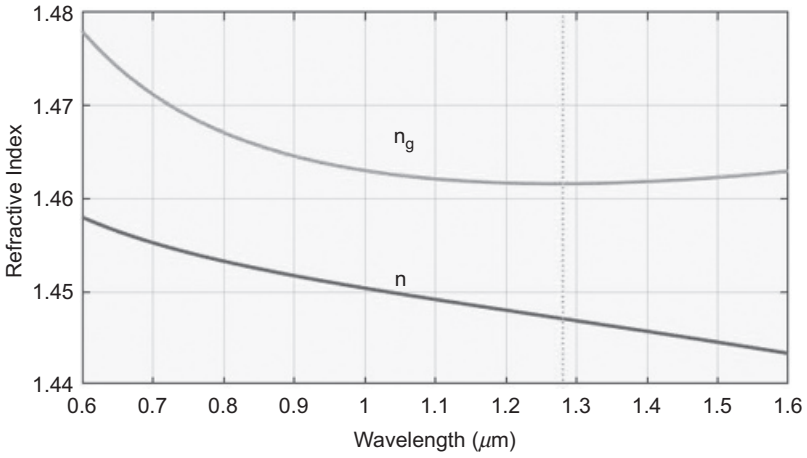

Figure 1.5 Variation of refractive index n and group index n_g with wavelength for fused silica. The dotted line indicates the zero-dispersion wavelength.

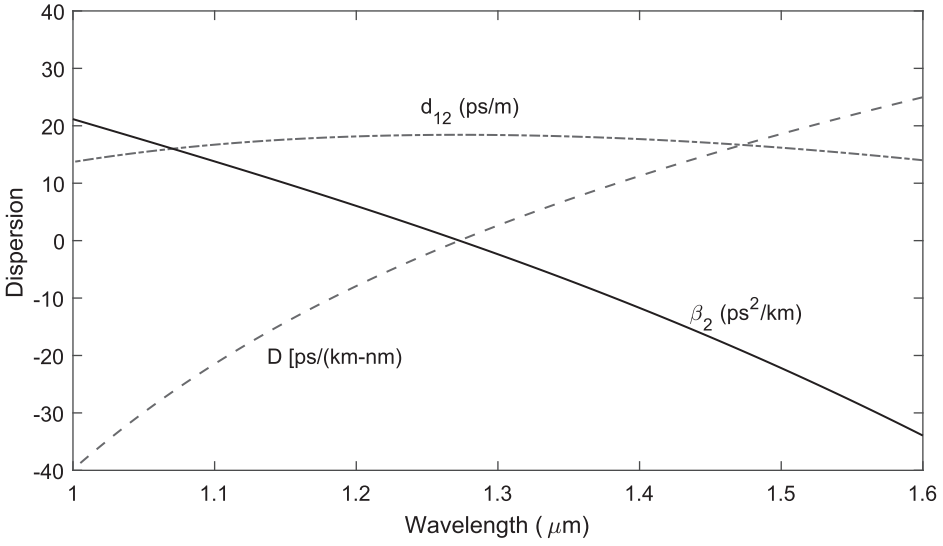

Figure 1.6 Wavelength dependence of β_2, D, and d_{12} for silica glass.

The situation changes considerably when silica glass is used to make a GRIN device. It will be seen in Chapter 2, that the propagation constant β, and hence all dispersion parameters, become mode-dependent for any GRIN medium. In particular, one must consider the intermodal group delay resulting from different values of β_1 for different modes. This topic is covered in Sections 2.4 and 4.1 in the context of optical pulses.

https://doi.org/10.1017/9781009282086.002 Published online by Cambridge University Press

1.3.3 Intensity Dependence of Refractive Index

The response of any dielectric to electromagnetic radiation becomes nonlinear for intense electric fields, and materials used for making GRIN devices are no exception. Several common nonlinear effects have their origin in the Kerr effect. According to it, the refractive index of any material increases at high intensities such that [28]

$$n(I) = n_0 + n_2 I, \tag{1.3.9}$$

where I is the local intensity and n_0 is the low-intensity value of the refractive index. The parameter n_2 is called the *Kerr coefficient*. Its numerical value depends on the material used to make a GRIN device and is about 3×10^{-20} m^2/W for silica glass.

Adding the nonlinear contribution, the refractive index of a GRIN medium has the form

$$n(\mathbf{r}, \omega, I) = n_0(\omega)[1 - \Delta f(\mathbf{r})] + n_2 I(\mathbf{r}), \tag{1.3.10}$$

where the dependence on all three variables is shown explicitly. The maximum value of the nonlinear contribution, $\delta n = n_2 I(\mathbf{r})$, occurs at the location where the intensity peaks. Denoting this peak value with $I_0 = P_0/A_e$, where P_0 is the peak power and A_e is the effective beam area, $\delta n = n_2 P_0/A_e$. As an example, if we use $A_e = 1$ cm^2 and $n_2 = 3 \times 10^{-20}$ m^2/W, $\delta n = 3 \times 10^{-13}$ even at a relatively high peak power of $P_0 = 1$ kW. This value is too small to have any impact when a CW beam is launched inside a GRIN rod.

There are two ways to enhance the nonlinear effects inside a GRIN medium. First, the beam's effective area A_e is reduced considerably when GRIN fibers are used with a core radius close to 10 μm. Second, if a beam containing a train of short optical pulses is used, the peak power P_0 of the pulse can exceed 1 MW. Using $A_e = 10^{-10}$ m^2 for a GRIN fiber, the nonlinear contribution to the refractive index (about 3×10^{-4}) is much smaller than Δ, indicating that it is not likely to affect the GRIN-induced self-imaging phenomenon discussed in Chapter 3. However, if the GRIN fiber is long enough, the nonlinear contribution can affect both the temporal and spectral features of a pulsed beam. As noted in Chapter 5, it also produces novel spatiotemporal features that have been studied extensively in recent years [19–21].

The intensity dependence of the refractive index leads to several nonlinear effects; the two most common ones are known as *self-focusing* and *self-phase modulation* (SPM). The phenomenon of self-focusing is relevant for GRIN media because it can compress an optical beam and compete with the GRIN-induced focusing. Moreover, it leads to a beam's collapse above a certain critical power level [28].

SPM is relevant only for pulsed optical beams. It produces a self-induced phase shift that is different for different parts of the same pulse because of its intensity dependence. Its magnitude can be obtained from Eq. (1.3.10). After a distance L,

the nonlinear phase shift is given by

$$\phi_{\mathrm{NL}}(\mathbf{r}, t) = (n_2 k_0 L) I(\mathbf{r}, t), \qquad k_0 = 2\pi/\lambda. \tag{1.3.11}$$

The phase shift depends both on the spatial location $\mathbf{r}$ and t because the intensity of a pulsed beam varies with time. This feature is called SPM because a pulse modifies its own phase. The spatial dependence produces a curved wavefront and leads to self-focusing when $n_2 > 0$ and self-defocusing when $n_2 < 0$. The time dependence produces spectral broadening of a pulsed beam [20]. It can also lead to the formation of optical solitons in the anomalous-GVD region of a GRIN fiber [29].

A related nonlinear phenomenon, known as cross-phase modulation (XPM), refers to the nonlinear phase shift of an optical field induced by another field having a different wavelength or state of polarization. Its origin can be understood by noting that the total electric field, in the case of two fields of different wavelengths but the same state of polarization, is given by

$$\mathbf{E}(\mathbf{r}, t) = \hat{\mathbf{x}} \mathrm{Re}[E_1 \exp(-i\omega_1 t) + E_2 \exp(-i\omega_2 t)]. \tag{1.3.12}$$

In this situation, the nonlinear phase shift at the frequency ω_1 is found to be [20]

$$\phi_{\mathrm{NL}} = n_2(\omega_1/c)L(|E_1|^2 + 2|E_2|^2). \tag{1.3.13}$$

The first term is the SPM term seen in Eq. (1.3.11). The second term is due to XPM because it represents a phase shift induced by another beam at a different wavelength. The Kerr effect also leads to four-wave mixing when a phase-matching condition is satisfied [20].

1.4 GRIN Materials and Fabrication

Both glasses and plastics are used for making GRIN devices, which are divided into two broad categories based on their transverse dimensions – GRIN rods and GRIN fibers. The radius a of the cylindrical region over which $n(\rho)$ varies exceeds 1 mm for GRIN rods. In contrast, a is restricted to values in the range of 10–30 μm for GRIN fibers. Silica glass is commonly used for making GRIN fibers, but GRIN rods can be made with other materials as well.

In spit of the amorphous nature of glass, its refractive index can be treated as being constant over lengths longer than a wavelength. Thus, glass in its natural state is a homogeneous medium. The important question is how one can modify the refractive index of a glass such that it varies in a prescribed manner with the distance ρ from the central axis. From a fundamental perspective, the refractive index of a material depends on its density and can only be changed by making its density nonuniform. As early as 1980, a review of the GRIN materials listed six

https://doi.org/10.1017/9781009282086.002 Published online by Cambridge University Press

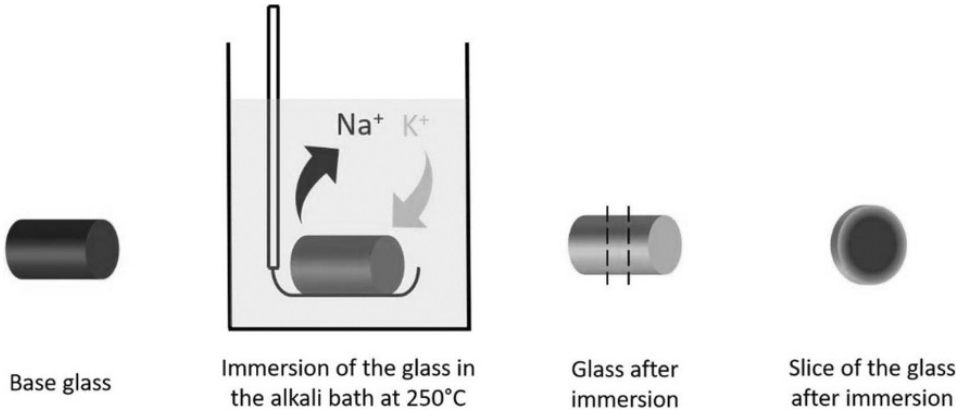

Figure 1.7 Schematic of the ion-exchange process used to make GRIN rods. (After Ref. [33]; ©2021 CC BY.)

different techniques developed for this purpose [30]. In one approach, a boron-rich glass rod is bombarded with neutrons. As neutrons enter the glass, its refractive index decreases because neutrons change the boron's concentration. The decrease is the largest in the outer region of the glass rod and becomes negligible near the rod's center, resulting in a gradient in the glass's refractive index.

Another common method is known as the ion-exchange technique [31–33]. In this approach, shown schematically in Figure 1.7, a base glass with heavier ions (such as K^+) is immersed into a molten salt bath containing lighter alkali ions. At a suitable temperature, lighter ions diffuse into the glass and replace the heavy ions present within the glass [4]. This ionic exchange creates a gradient in the refractive index of the glass because fewer and fewer ions are replaced as one moves from the outer surface toward the central region of the glass. Diffusion of ions into the glass is affected by several factors, such as the strength of bonds that hold the glass ions in their lattice sites and the relative mobilities of various ions inside the glass network. As the mobility of ions depends on temperature, a higher temperature helps in practice. An external electric field is also used to speed up the ion-exchange process and to control the shape of the resulting refractive-index profile [34].

An ion-stuffing technique has also been used for making GRIN devices. In this case, a special glass is chosen whose structure (or phase) changes when heated suitably. The changed part is soluble in a specific acid. When the glass is immersed in this acid, the diffusion of acid into the glass removes less and less material from the inner regions of the glass, resulting in the formation of an index gradient. The main issue with this technique is that very few glasses exist that exhibit phase separation, and the phase separation is not always uniform.

A different technique, known as chemical vapor deposition (CVD), is employed

https://doi.org/10.1017/9781009282086.002 Published online by Cambridge University Press

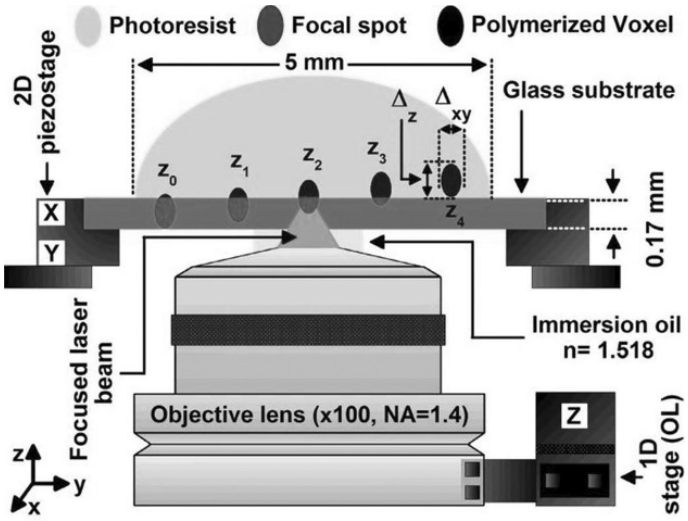

Figure 1.8 Schematic of the direct laser writing scheme used for making GRIN devices. (After Ref. [38]; ©2020 CC BY.)

for making GRIN fibers [35]. The fabrication of such fibers involves two stages. First, a cylindrical rod of about 2 cm diameter is produced with the desired refractive-index profile by depositing silica, layer by layer, inside of a silica tube. An index-increasing dopant material (such as germania) is added to each layer such that the density of dopants varies from one layer to another and is larger in the central region of the tube [36]. The resulting structure is called a preform, which is drawn into the form of a GRIN fiber using a draw tower. Both fabrication stages involve sophisticated technology to ensure the uniformity of the index profile within the fiber's core. A polymerization technique can also be used when a plastic material is used for making GRIN fibers [13]. In this approach, the monomer of an organic material is differentially changed into a polymer by irradiation of ultraviolet radiation.

A technique called *direct laser writing* has been developed in recent years [37–39]. As shown in Figure 1.8, it uses point-by-point exposure of a plastic material to intense laser pulses to change its local refractive index through polymerization. The exposure dose is varied during scanning by varying the laser's power to produce an index gradient. This technique employs a lithographic approach in the sense that an arbitrary refractive-index profile can be created by using a photoresist that is exposed to laser pulses, which modify the refractive index through a multiphoton polymerization process [39].

A nanoscale engineering technique was used in 2018 for making GRIN fibers [40]. In this approach, the core of the preform is made by combining two types of glass rods, made of pure silica and Ge-doped silica, in such a fashion that the density

https://doi.org/10.1017/9781009282086.002 Published online by Cambridge University Press

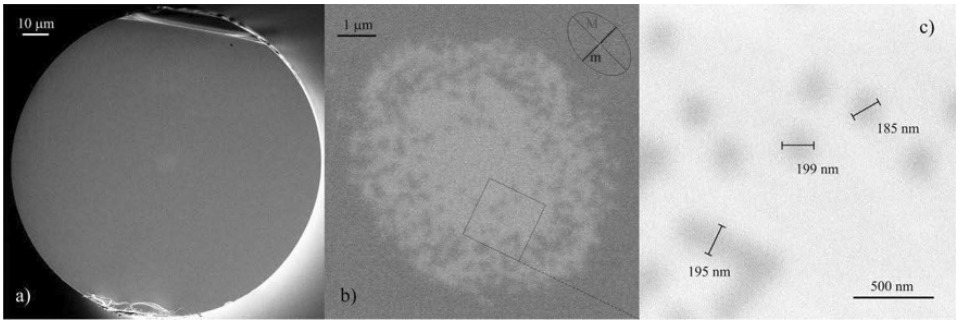

Figure 1.9 SEM images at three magnification levels of a GRIN finer made with the nanoscale engineering technique. (After Ref. [40]; ©2018 CC BY.)

of Ge-doped rods is the largest near the core's center and decreases gradually as the radial distance increases. As a result, the refractive index is effectively graded inside the fiber's core when the preform is drawn into a thin fiber. This technique was used to produce a GRIN fiber with a parabolic index profile. A preform was first made by stacking more than 2100 rods with a core diameter of 0.45 mm inside a tube of silica glass (see Figure 10.8 of Chapter 10). The fiber was drawn using this preform until the diameter of each rod was reduced to nearly 190 nm. Figure 1.9 shows images of this fiber's cross section at three magnification levels that were obtained with a scanning electron microscope (SEM). Part (a) shows the whole fiber, part (b) shows its core, and part (c) shows individual nanosize rods within the core. Such a nanostructure-based technique is not limited to the circular geometry and is flexible enough to produce GRIN fibers with any index profile.

1.5 Overview of Book's Contents

This book provides a comprehensive coverage of the physics of optical phenomena inside a GRIN medium and uses it for understanding the operation of engineered devices such as GRIN lenses, sensors, endoscopes, and tweezers. The first chapter begins with a historical perspective and introduces different refractive-index profiles that can be employed for making a GRIN device. It also focuses on the relevant properties of a GRIN medium, such as power loss, chromatic dispersion, and intensity dependence of the refractive index at high power levels, which may affect the operation of practical devices. The techniques used to fabricate GRIN devices are also discussed in this chapter.

Chapter 2 starts with Maxwell's equations and uses them to obtain the wave equation that must be solved to understand the propagation of optical waves inside a GRIN medium. This equation is solved in Section 2.2 to obtain the modes of a

https://doi.org/10.1017/9781009282086.002 Published online by Cambridge University Press

GRIN medium for a parabolic index profile. Non-parabolic profiles are considered in Section 2.3. When an optical beam is launched into a GRIN medium, it excites different modes with different efficiencies. This issue is discussed in Section 2.4, where we also consider multimode interference and intermodal dispersion. Section 2.5 describes several non-modal techniques that can be used for studying wave propagation in GRIN media.

The focus of Chapter 3 is on the focusing and self-imaging of optical beams inside a GRIN medium. Section 3.1 provides a geometrical-optics perspective and shows why optical rays follow a curved path inside a GRIN medium. The modal expansion is used in Section 3.2 to obtain a propagation kernel that can be used for beams of any spatial shape. It is used to discuss the self-imaging phenomenon. It is also used to study the propagation of Gaussian beams launched on-axis, or offset from the central axis of a GRIN medium. Section 3.3 is devoted to studying how a GRIN rod can be used as a flat lens to focus or to collimate a beam. Imaging characteristics of such a lens are also studied in this section. Several important applications of GRIN devices are discussed in Section 3.4.

Chapter 4 is devoted to the study of the dispersive effects that affect a pulsed beam propagating inside a GRIN medium. In Section 4.1, an equation governing the evolution of optical pulses is obtained. The dispersion parameters appearing in this equation change, depending on which mode is being considered. Section 4.2 focuses on the distortion of optical pulses resulting from differential group delay and group-velocity dispersion. Section 4.3 deals with the effects of linear coupling among the modes occurring because of random variations in the core's shape and size along the fiber's length. A non-modal approach is developed in Section 4.4 for short optical pulses propagating inside a GRIN medium. Section 4.5 describes important applications such as optical communications and biomedical imaging.

The focus of Chapter 5 is on the intensity dependence of the refractive index that leads to a variety of interesting nonlinear effects in the case of GRIN fibers. We consider in Section 5.1 the self-focusing of a CW beam inside a GRIN medium. The pulsed beams are considered in Section 5.2, where we discuss the phenomena of self- and cross-phase modulations. Section 5.3 is devoted to the modulation instability and the formation of multimode solitons. Intermodal nonlinear effects are described in Section 5.4 with emphasis on four-wave mixing and stimulated Raman scattering. Applications such as supercontinuum generation and spatial beam cleanup are discussed in Section 5.5.

Chapter 6 is devoted to the effects related to the presence of loss or gain inside a GRIN medium. Loss is considered in Section 6.1. Except for a reduced power level, its effects are found to be relatively minor. We discuss in Section 6.2 the mechanisms used for providing optical gain inside an active GRIN medium. Section 6.3 is devoted to Raman amplifiers and lasers, built with GRIN fibers and pumped suitably to

provide the optical gain. Parametric amplifiers are discussed in Section 6.4, together with the phase matching required for four-wave mixing to occur inside them. The focus of Section 6.5 is on amplifiers and lasers made by doping a GRIN fiber with rare-earth ions. Section 6.6 includes the nonlinear effects and describes how spatial solitons and similaritons can form under suitable conditions inside an active GRIN medium.

Chapter 7 focuses on a nonuniform GRIN fiber, tapered to induce variations in the refractive index along its length, in addition to the transverse radial variations. Section 7.1 describes the ray-optics and wave-optics techniques that can be used for studying propagation of optical beams inside such a medium. Section 7.2 discusses the impact of tapering on the periodic self-imaging for several different tapering profiles. The analogy between a GRIN medium and a harmonic oscillator is exploited in Section 7.3, where we discuss several quantum-mechanical techniques. Section 7.4 is devoted to the case of periodic axial variations, induced by changing the core's radius in a periodic fashion.

Chapter 8 is devoted to the formation of optical vortices inside a GRIN medium. After discussing important polarization concepts in Section 8.1, we use in Section 8.2 specific combinations of the modes that act as vortices with different states of polarizations. Cylindrical vector beams with radial or azimuthal polarization are also discussed. In Section 8.3, we present the techniques used for generating different types of vortex beams. Section 8.4 shows that vortex beams also exhibit the self-imaging property during their propagation inside a GRIN medium. The impact of random mode-coupling is also discussed in this section. Vortex-based applications of GRIN fibers are covered in Section 8.5.

The focus of Chapter 9 is on photonic spin-orbit coupling occurring inside a GRIN medium. Section 9.1 describes two physical mechanisms that can produce changes in the states of polarization of an optical beam. The exact wave equation with the term involving the index gradient is solved in Section 9.2 to introduce the path-dependent geometrical phase to discuss the photonic analog of the spin-Hall effect and conversion between the spin and orbital angular momenta. Section 9.3 considers how the scalar LP_{lm} modes change when the index-gradient term is taken into account. A quantum approach is employed in Section 9.4 to find the exact vector modes of a GRIN medium.

Chapter 10 is devoted to two research areas that have attracted considerable attention in recent years – photonic crystals and metamaterials. Both are artificial structures made by combining two or more materials on a subwavelength scale. They can also be used to make GRIN devices with a spatially varying refractive index. Section 10.1 introduces the basic concepts needed to understand the physics behind the photonic crystal and metamaterials. Section 10.2 is devoted to the engineering of GRIN structures based on photonic crystals. Section 10.3 deals

with the metamaterial-based GRIN devices, while the GRIN devices based on metasurfaces are discussed in Section 10.4.

The focus of Chapter 11 is on studying the impact of fluctuations in the amplitude or phase of an optical beam propagating inside a GRIN medium. Such beams are called partially coherent. Section 11.1 introduces the basic concepts related to the topic of partial coherence. Section 11.2 considers how the self-imaging phenomenon is affected by the partial coherence of an incoming beam. The evolution of a partially coherent beam inside a GRIN medium is studied in Section 11.3 using its cross-spectral density. The general result is used to discuss changes in the intensity, optical spectrum, and the degree of spatial coherence. The focus of Section 11.4 is on the polarization effects associated with a partially coherent beam. The concept of polarization matrix is used to discuss periodic changes occurring both in the state of polarization and the degree of polarization.

References

[1] J. C. Maxwell, *The Scientific Papers of James Clerk Maxwell*, vol. 1, ed., W. D. Niven (Cambridge University Press, 1890), 76–79.

[2] R. W. Wood, *Phil. Mag. J. Sci.*, Series 6, **12**, 159 (1906); https://doi.org/10.1080/14786440609463529.

[3] R. K. Luneburg, *Mathematical Theory of Optics* (Brown University, 1944).

[4] A. D. Pearson, W. G. French, and E. G. Rawson, *Appl. Phys. Lett.* **15**, 76 (1969); https://doi.org/10.1063/1.1652909.

[5] T. Uchida, M. Furukawa, I. Kitano, K. Koizumi, and H. Matsumura, *IEEE J. Quantum Electron.* **6**, 606 (1970); https://doi.org/10.1109/JQE.1970.1076326.

[6] T. Izawa and H. Nakagome, *Appl. Phys. Lett.* **21**, 584 (1972); https://doi.org/10.1063/1.1654265.

[7] I. P. Kaminow and J. R. Carruthers, *Appl. Phys. Lett.* **22**, 326 (1973); https://doi.org/10.1063/1.1654657.

[8] H. Smithgall and F. W. Dabby, *IEEE J. Quantum Electron.* **9**, 1023 (1973); https://doi.org/10.1109/JQE.1973.1077405.

[9] M. S. Sodha and A. K. Ghatak, *Inhomogeneous Optical Waveguides* (Plenum Press, 1977).

[10] E. W. Marchand, *Gradient Index Optics* (Academic Press, 1978).

[11] R. Olshansky, *Rev. Mod. Phys.* **51**, 341 (1979); https://doi.org/10.1103/RevModPhys.51.341.

[12] G. P. Agrawal, *Fiber-Optic Communication Systems*, 5th ed. (Wiley, 2021).

[13] Y. Koike, *Fundamentals of Plastic Optical Fibers* (Wiley, 2014).

[14] Special issues of Applied Optics publsihed on April 1, 1980, March 15, 1982, February 1, 1983, June 1, 1984, December 15, 1985, October 1, 1986, February 1, 1988, October 1, 1990, December 1, 1990, and September 1, 1992.

[15] Y. A. Kravtsov and Y. I. Orlov, *Geometrical Optics of Inhomogeneous Media* (Springer, 1990).

[16] C. Gomez-Reino, M. V. Perez, and C. Bao, *Gradient Index Optics: Fundamentals and Applications* (Springer, 2003).

[17] D. J. Richardson, J. M. Fini, and L. E. Nelson, *Nat. Photon.* **7**, 354 (2013); https://doi.org/10.1038/nphoton.2013.94.
[18] T. Mizuno, H. Takara, A. Sano, and Y. Miyamoto, *J. Lightwave Technol.* **34**, 1484 (2016); https://doi.org/10.1109/JLT.2016.2615070.
[19] K. Krupa, V. Couderc, A. Tonello et al., Spatiotemporal Nonlinear Dynamics in Multimode Fibers, in *Nonlinear Guided Wave Optics*, Ed. S. Wabnitz (IOP Science, 2017), 14-1 to 14-23.
[20] G. P. Agrawal, *Nonlinear Fiber Optics*, 6th ed. (Academic Press, 2019), 621-683.
[21] K. Krupa, A. Tonello, A. Barthélémy et al., *APL Photon.* **4**, 110901 (2019); https://doi.org/10.1063/1.5119434.
[22] A. Ghatak and K. Thyagarajan, *An Introduction to Fiber Optics* (Cambridge University Press, 1998).
[23] J. A. Buck, *Fundamentals of Optical Fibers*, 2nd ed. (Wiley, 2004).
[24] K. Okamoto, *Fundamentals of Optical Waveguides*, 2nd ed. (Academic Press, 2010).
[25] M. Born and E. Wolf, *Principles of Optics*, 7th ed. (Cambridge University Press, 2020).
[26] N. Ioannides, E. B. Chunga, A. Bachmatiuk et al., *Mater. Res. Express* **1**, 032002 (2014); https://doi.org/10.1088/2053-1591/1/3/032002.
[27] I. H. Malitson, *J. Opt. Soc. Am.* **55**, 1205 (1965); https://doi.org/10.1364/JOSA.55.001205.
[28] R. W. Boyd, *Nonlinear Optics*, 4th ed. (Academic Press, 2020).
[29] A. S. Ahsan and G. P. Agrawal, *Opt. Lett.* **43**, 3345 (2018); https://doi.org/10.1364/OL.43.003345.
[30] D. T. Moore, *Appl. Opt.* **19**, 1035 (1980); https://doi.org/10.1364/AO.19.001035.
[31] J. R. Hensler, U.S. Patent 3,873,408 (1975); https://patents.google.com/patent/US3873408A/en.
[32] R. V. Ramaswamy and R. Srivastava, *J. Lightwave Technol.* **6**, 984 (1988); https://doi.org/10.1109/50.4090.
[33] C. Fourmentin, X. H. Zhang, E. Lavanant et al., *Sci. Rep.* **11**, 11081 (2021); https://doi.org/10.1038/s41598-021-90626-4.
[34] S. N. Houde-Walter and D. T. Moore, *Appl. Opt.* **24**, 4326 (1985); https://doi.org/10.1364/AO.24.004326.
[35] D. B. Keck and R. Olshansky, U.S. Patent 3,904,268 (1975); https://patents.google.com/patent/US3904268A/en.
[36] T. Izawa and S. Sudo, *Optical Fibers: Materials and Fabrication* (Springer, 1987).
[37] A. Zukauskas, I. Matulaitiene, D. Paipulas et al., *Laser Photon. Rev.* **9**, 1863 (2015); https://doi.org/10.1002/lpor.201500170.
[38] Y. Bougdid and Z. Sekkat, *Sci. Rep.* **10**, 10409 (2020); https://doi.org/10.1038/s41598-020-67184-2.
[39] C. R. Ocier, C. A. Richards, D. A. Bacon-Brown et al., *Light Sci. Appl.* **9**, 196 (2020); https://doi.org/10.1038/s41377-020-00431-3.
[40] A. Anuszkiewicz, R. Kasztelanic, A. Filipkowski et al., *Sci. Rep.* **8**, 1 (2018); https://doi.org/10.1038/s41598-018-30284-1.